램제트 엔진의 비정상 천이 유동에 관한 연구

성 홍 계* · Vigor Yang**

Unsteady Transient Flowfield in an Integrated Rocket Ramjet Engine

H.K.Sung* · Vigor Yang**

ABSTRACT

A numerical analysis has been conducted to study the transient flowfield during the transition from the booster to sustainer phase in an integrated rocket ramjet (IRR) propulsion system. Emphasis is placed on the unsteady inlet aerodynamics, fuel/air mixing in an entire ramjet engine during the flow transient phase. The computational geometry consists of the entire IRR engine, including the inlet, the combustion chamber, and the exhaust nozzle. Turbulence closure is achieved using a low-Reynolds-number - two-equation model. The governing equations are solved numerically by means of a finite-volume, preconditioned flux-differencing scheme over a wide range of Mach number. Various important physical processes are investigated systemically, including terminal shock train.

Nomenclature

$a_1, a_2, \ldots$ empirical constants
C_p species specific heat at constant pressure
C_μ empirical constants
C_1, C_2 empirical constants
c speed of sound
E specific total energy or x-directional convective-flux vector
E_i activation energy of reaction I
Ev x-directional diffusion-flux vector
F y-directional convective-flux vector
Fv y-directional diffusion-flux vector
f frequency
f_μ damping factor
H source term vector
h specific enthalpy of mixture
I imaginary part of complex
k turbulence kinetic energy
k_{fi} reaction rate constants of the forward reactions

*국방과학연구소
**The Pennsylvania State University

k_{bi} reaction rate constants of the backward reactions
L total number of reaction step
MW_k molecular weight of species k
N total number of species
p pressure
Q conserved variable vector
q_i the heat flux vector
R_e Reynolds number
R_u universal gas constant
S flame speed
S_{xy} two-sided, cross-spectral density function f x and y
T temperature
t time
U_k diffusion velocity of species k
u velocity
x spatial coordinate
Y_k mass fraction of species k
y^+ variable distance from wall
Z pseudo-time variable vector

Greek Symbols

β scaling factor
χ_k molar concentration of species k
Δ forward difference or filter width
ϵ turbulence dissipation rate
ψ quivalence ratio
Γ preconditioning matrix
λ heat conductivity
μ viscosity
τ_{ij} viscous stress tensor for a Newtonian gas
ν'_{ki} stoichiometric coefficients on the reactants side for species k in the ith reaction
ν''_{ki} stoichiometric coefficients on the products side for species k in the ith reaction
θ phase angle
ρ density
σ_k empirical constant
σ_ε empirical constant
τ pseudo-time
τ_t turbulent time scale
τ_k olmogorov time scale
$\dot{\omega}$ net production rate of chemically reaction

Subscripts

av average value
f formation
i spatial coordinate or reaction step index
j spatial coordinate index
k spatial coordinate or species index
L laminar property
M model value of experiment
p pressure or index of polynomial function
R reference value
rms root mean square
t turbulent property
u unburned fuel
v viscous

Superscripts

T transpose of vector or temperature
$'$ fluctuation

I. Introduction

An integrated rocket ramjet (IRR) combines a rocket booster and a ramjet sustainer in one efficient propulsion system with a common combustion chamber for both the boost and sustain phases. This concept yields a much more compact design than previous rocket/ramjet systems such as a ramjet with a tandem booster rocket that is jettisoned

after burnout. The large difference in chamber operating pressure between the rocket booster (about 100 atmospheres) and the ramjet sustainer (around 6 atmospheres at cruising flight) phases is a major IRR design problem, which has been handled by using an ejectable booster nozzle ejected after the boost phase. However, this system creates additional reliability problems such as dynamic impact on the vehicle during ejection of the booster nozzle and transition time delay from the booster to the ramjet sustainer. A nozzleless booster, utilizing the propellant grain as a nozzle, circumvents the inherent problem of an ejectable nozzle system.1 During rocket operation, the combustor functions as a conventional rocket combustor, closed at the forward end, with a suitable nozzle formed from the propellant grain at the aft end. During transition, the combustion chamber must reconfigure itself for the ramjet operation, open at the forward end to allow the ram air to enter the combustor, and with a large throat nozzle at the aft end, suitable for ramjet operation, as illustrated in Fig. 1.2

The port cover, which seals the upstream end of the combustion chamber, is ruptured at the end of the boost phase to allow ram air to enter the chamber for the sustainer phase. The design of a port cover must consider quick and reliable transition without damaging the combustor hardware. After the tail-off of the booster thrust, drag force acting on an airframe causes the ramjet to rapidly lose the forward speed, typically on the order of Mach numbers 0.1 per second.2 A longer transition time requires increased booster loading, which reduces the amount of ramjet fuel that can be carried on board, and consequently shortens the flight range of the vehicle. Hence, the transition to ramjet take-over must be accomplished in a timely fashion. When the pressure in the booster rocket chamber decays to a value where positive vehicle acceleration approaches zero, the inlet port-cover separation system operates. The port cover is forced into the combustor when the inlet ram air pressure exceeds the residual chamber pressure. The cover is expelled through the ramjet nozzle by the force of the incoming ram air. Inside the combustor, the ram air is decelerated and pushes out the hot gases from the booster phase. The recirculating flow downstream of the dump plane aids in the ignition of the injected ramjet fuel, as does the remaining residuals of both the rocket propellant grain and the thermal protection system combustibles. Reliable ignition and stable burning of the ramjet fuel during this transient phase are important concerns, complicated by uncertainties such as the mass flow rate and velocity of the ram air, fuel mixing, ignitionability of fuel, flame holding, and so on.

Since French engineer Rene Lorin first introduced the ramjet engine concept in 1913, substantial research has been pursued to understand ramjet internal flows, especially in the areas of supersonic inlet dynamics and combustion instability. Notable are the numerical and experimental investigations of unsteady diffuser flowfield discussed in Refs. 3-14 and longitudinal combustion oscillations addressed in Refs. 15-26. All of these efforts were motivated to improve the knowledge base of low-frequency combustion instability and its an inlet flows. However, the previous studies except the work by Hsieh23 and Sung24~26 focused on either the inlet or combustor under quasi-steady operating conditions; the direct computing between the

two subsystems was ignored in spite of its significance in determining the overall engine dynamics. The purpose of the present work is to conduct a unified analysis, which allows for a complete treatment of the engine flow development, ranging from the leading edge of the inlet center body through the exhaust nozzle.

The major issues in this paper are :

- How the flow field is established on placing an inlet port cover between the diffuser and the combustion chamber.
- Shock trains just after removing the port cover.
- The shock and boundary layer interaction, and vortices behaviors.
- Interaction of cold ram air and hot booster rocket gas.

II. Theoretical Formulation

A. Governing Equations

The governing equations based on the conservation of mass, momentum and energy, and species concentration for a compressible, chemically reacting gas can be written as

$$\frac{\partial \rho}{\partial t} + \frac{\partial \rho u_j}{\partial x_j} = 0 \tag{1}$$

$$\frac{\partial \rho u_i}{\partial t} + \frac{\partial (\rho u_i u_j + p\delta_{ij})}{\partial x_j} = \frac{\partial \tau_{ij}}{\partial x_j} \tag{2}$$

$$\frac{\partial \rho E}{\partial t} + \frac{\partial ((\rho E + p)u_j)}{\partial x_j} = \frac{\partial (u_i \tau_{ij} - q_j)}{\partial x_j} \tag{3}$$

$$\frac{\partial \rho Y_k}{\partial t} + \frac{\partial \rho Y_k u_j}{\partial x_j} = \dot{\omega}_k - \frac{\partial \rho Y_k U_{k,j}}{\partial x_j}, \quad k = 1, \ldots, N \tag{4}$$

Standard notations in fluid mechanics are used, with repeated indices implying summation over the axial and radial components. The viscous stress tensor τ_{ij} for a Newtonian gas and the heat flux vector q_j are, respectively,

$$\tau_{ij} = (\mu_m + \mu_t)\left(\frac{\partial u_i}{\partial x_j} + \frac{\partial u_j}{\partial x_i} - \frac{2}{3}\delta_{ij}\frac{\partial u_l}{\partial x_l}\right) \tag{5}$$

$$q_j = -(\lambda_m + \lambda_t)\frac{\partial T}{\partial x_j} + \rho \sum_{k=1}^{N} h_k Y_k U_{k,j} \tag{6}$$

The specific total energy E is given:

$$E = h - \frac{p}{\rho} + \frac{u_j u_j}{2} \tag{7}$$

The specific enthalpy of mixture, h, contains contributions from its constituent species such as:

$$h = \sum_{k=1}^{N} Y_k h_k = \sum_{k=1}^{N} Y_k \left(\Delta h^{\circ}_{f,k} + \int_{T_{ref}}^{T} C_{p,k}(T')\, dT' \right) \tag{8}$$

The species specific heat at constant pressure, $C_{p,k}$, can be approximated by a polynomial function of temperature such as:

$$C_{p,k} = \sum_{p=1}^{M} a_{k,p} T^{p-1} \tag{9}$$

The formulation is closed by an equation of state for a perfect mixture such as :

$$p = \rho R_u T \sum_{k=1}^{N} \frac{Y_k}{W_k} \tag{10}$$

The following relation expresses the net production rate ($\dot{\omega}$) of each species in a multi-step mechanism:

$$\dot{\omega}_k = MW_k \sum_{i=1}^{I} (\nu''_{ki} - \nu'_{ki}) \left[k_{fi} \prod_{k=1}^{N} [\chi_k]^{\nu'_{ki}} - k_{bi} \prod_{k=1}^{N} [\chi_k]^{\nu''_{ki}} \right] \quad for \quad k = 1, 2, \ldots, N \tag{11}$$

B. Turbulence Closure

The standard k-ε model was proposed for high Reynolds number flows and is traditionally used with a wall function and

the variable $y+$ as a damping function. Universal wall functions do not exist in complex flows, however, and the damping factor cannot be applied to flows with separation. Thus, a low Reynolds number k-ε model was developed for near-wall turbulence by Jones and Launder.[28] Shih and Lumley[29] observed that within certain distances from the wall, all energetic large eddies will reduce to Kolmogorov eddies (the smallest eddies in turbulence), and all the important wall parameters, such as friction velocity, viscous length scale, and mean strain rate at the wall, can be characterized by the Kolmogorov micro scale.

Yang and Shih30 proposed a time-scale-based k-ε model for the near-wall turbulence related to the Kolmogorov time scale as its lower bound, so that the equation can be integrated to the wall. The advantages of this model are (a) no singularity at the wall, and (b) adaptability to separation flow, since the damping function is based on the Reynolds number instead of $y+$. The low Reynolds number models have been designed to maintain the high Re formulation in the log-law region and further tuned to fit measurements for the viscous and buffer layers. The low Reynolds number model used in this work is based on Yang and Shih[27]. In the bulk flow region, the distributions of the turbulence kinetic energy k and its dissipation rate are calculated from the following transport equations :

$$\frac{\partial \rho k}{\partial t}+\frac{\partial(\rho u_j k)}{\partial x_j}=\frac{\partial}{\partial x_j}\left(\left(\nu+\frac{\nu_T}{\sigma_k}\right)\frac{\partial k}{\partial x_j}\right)+S_k \tag{12}$$

$$\frac{\partial \rho \varepsilon}{\partial t}+\frac{\partial(\rho u_j \varepsilon)}{\partial x_j}=\frac{\partial}{\partial x_j}\left(\left(\nu+\frac{\nu_T}{\sigma_\varepsilon}\right)\frac{\partial \varepsilon}{\partial x_j}\right)+S_\varepsilon \tag{13}$$

where

$$S_k=\mu_T\left(\left(\frac{\partial u_i}{\partial x_j}+\frac{\partial u_j}{\partial x_i}\right)-\frac{2}{3}\rho k\delta_{ij}\right)\frac{\partial u_i}{\partial x_j}-\rho\varepsilon \tag{14}$$

$$S_\varepsilon=\left(C_{1\varepsilon}\mu_T\left(\left(\frac{\partial u_i}{\partial x_j}+\frac{\partial u_j}{\partial x_i}\right)-\frac{2}{3}\rho k\delta_{ij}\right)\frac{\partial u_i}{\partial x_j}-C_{2\varepsilon}\rho\varepsilon\right)/T_t+\Lambda \tag{15}$$

$$\Lambda=\nu\mu_t\left(\frac{\partial u_i}{\partial x_j\partial x_k}\right)^2 \tag{16}$$

$$\sigma_k = 1.0$$

$$\sigma_\varepsilon = 1.3$$

It is noted that the above empirical constants (σ_k, σ_ε) are identical to those of the standard k-ω model.

The turbulent viscosity is determined from the following relation

$$\mu_t=\rho C_\mu f_\mu k\tau_t \tag{17}$$

where is the turbulent time scale defined as

$$\tau_t=\frac{k}{\varepsilon}+\tau_k \tag{18}$$

and τ_k is the Kolmogorov time scale defined as

$$\tau_k=C_k\left(\frac{\nu}{\varepsilon}\right)^{1/2} \tag{19}$$

The damping factor $f\mu$ is used to account for the wall effect

$$f_\mu=[1-\exp(-a_1R_y-a_3R_y^3-a_5R_y^5)]^{1/2} \tag{20}$$

where

$$R_y=k^{1/2}y_n/\nu \tag{21}$$

The empirical constants in the above equations are recommended[30] as follows :

$C\mu = 0.09,\ C_1 = 1.44,\ C_2 = 1.92,$
$a_1 = 1.5\times10^{-4},\ a_3 = 5.0\times10^{-7},\ a_5 = 1.0\times10^{-10}$

Ⅲ. Numerical Formulation

The conservation equations for moderate and high Mach number flows are well coupled, and standard numerical techniques perform adequately. In regions of low Mach number flows, however, the energy and momentum equations are practically decoupled and the system of conservation equations becomes stiff. In the entire ramjet engine, the flow fields are governed by a wide variety of time scales (from supersonic flow in the inlet to almost stagnation-flow near the backward-step corner of the combustor). Such a wide range of time scales causes an unacceptable convergence problem in the case of unsteady calculations. Particularly, in regions with strong grid stretching or with low Mach number flows, the convergence may be severely impaired.

To overcome the problem, a dual time-integration procedure designed for all Mach number flows is applied. The pseudo-time derivative may be chosen to optimize the convergence of the inner iterations through using an appropriate preconditioning matrix that is tuned to rescale the eigenvalues to render the same order of magnitude to maximize convergence. To unify the conserved flux variables, a pseudo-time derivative of the form can be added to the conservation equation. Since the pseudo-time derivative term disappears as converged, a certain amount of liberty exists in choosing the variable Z. We take advantage of this by introducing a pressure as the pseudo-time derivative term in the continuity equation.

With the inclusion of the pseudo-time derivative term and the preconditioning matrix, the two dimensional axi-symmetric governing equation becomes

$$\Gamma\frac{\partial Z}{\partial\tau}+\frac{\partial Q}{\partial t}+\frac{\partial(E-E_v)}{\partial x}+\frac{\partial(F-F_v)}{\partial y}=H \tag{22}$$

The pseudo-time variable vector, Z, and its associated preconditioning matrix, Γ, may be taken as

$$Z=(p',u,v,h,Y_i)^T \tag{23}$$

$$\Gamma=\begin{pmatrix} 1/\beta & 0 & 0 & 0 & 0 & 0 & 0 & \cdots & 0\\ u/\beta & \rho & 0 & 0 & 0 & 0 & 0 & \cdots & 0\\ v/\beta & 0 & \rho & 0 & 0 & 0 & 0 & \cdots & 0\\ h_t\beta-1 & \rho u & \rho v & \rho & 0 & 0 & 0 & \cdots & 0\\ k/\beta & 0 & 0 & 0 & \rho & 0 & 0 & \cdots & 0\\ \varepsilon/\beta & 0 & 0 & 0 & 0 & \rho & 0 & \cdots & 0\\ Y_1/\beta & 0 & 0 & 0 & 0 & 0 & \rho & \cdots & 0\\ \cdot & \cdot & \cdot & \cdot & \cdot & \cdot & \cdot & \cdots & \cdot\\ \cdot & \cdot & \cdot & \cdot & \cdot & \cdot & \cdot & \cdots & \cdot\\ \cdot & \cdot & \cdot & \cdot & \cdot & \cdot & \cdot & \cdots & \cdot\\ Y_{N-1}/\beta & 0 & 0 & 0 & 0 & 0 & 0 & \cdots & \rho \end{pmatrix} \tag{24}$$

Also the scaling factor can be taken as:

$$\beta=\begin{cases} u_R^2, & \text{if } u^2<u_R^2\\ u^2, & \text{if } u_R^2<u^2<c^2\\ c^2, & \text{if } u^2>c^2 \end{cases} \tag{25}$$

The above variable vector are defined below:

$$Q=y\left[\rho,\rho u,\rho v,\rho E,\rho Y_k,\rho k,\rho\varepsilon\right]^T \tag{26}$$

$$E=y\left[\rho u,\rho u^2+p',\bar{\rho}uv,(\rho e+p)u,\rho uY_k,\rho uk,\rho u\varepsilon\right]^T \tag{27}$$

$$F=y\left[\rho v,\rho uv,\rho v^2+p',(\rho e+p)v,\rho vY_k,\rho vk,\rho v\varepsilon\right]^T \tag{28}$$

$$E_v=y\left[0,\tau^{xx},\tau^{xy},u\tau^{xx}+v\tau^{xy}-q^x,q^{kx},\left(\mu^m+\frac{\mu^t}{\sigma_k}\right)\frac{\partial k}{\partial x},\left(\mu^m+\frac{\mu^t}{\sigma_\varepsilon}\right)\frac{\partial\varepsilon}{\partial x}\right]^T \tag{29}$$

$$F = y\left[0, \tau_{xx}, \tau_{xy}, u\tau_{xy} + v\tau_{yy} - q_y, q_{by}, \left(\mu_m + \frac{\mu_t}{\sigma_t}\right)\frac{\partial k}{\partial y}, \left(\mu_m + \frac{\mu_t}{\sigma_\varepsilon}\right)\frac{\partial \varepsilon}{\partial y}\right]^T \tag{30}$$

$$H = \begin{bmatrix} 0 \\ -\frac{2}{3}\frac{\partial(\mu v)}{\partial x} \\ p' - \frac{4}{3}\frac{\mu v}{y} + \frac{2}{3}\mu\frac{\partial u}{\partial x} - \frac{2}{3}v\frac{\partial \mu}{\partial y} \\ -\frac{2}{3}\frac{\partial(\mu u v)}{\partial x} - \frac{2}{3}\frac{\partial(\mu v^2)}{\partial y} \\ y\delta_t \\ y(P_k - \rho\varepsilon) - \delta\left(\frac{2}{3}\mu_t v\left(\frac{\partial u}{\partial x} + \frac{\partial v}{\partial y}\right)\right) \\ y((C_{1\varepsilon}P_k - C_{2\varepsilon}\rho\varepsilon)/\tau_t + \Lambda) - \delta\left(\frac{2}{3}\mu_t v\left(\frac{\partial u}{\partial x} + \frac{\partial v}{\partial y}\right)C_{1\varepsilon}/\tau_t\right) \end{bmatrix} \tag{31}$$

The viscosity μ consists of both molecular (μ_m) and eddy viscosity (μ_t), (i.e., $\mu = \mu_m + \mu_t$).

The conservation equations, including finite chemical reactions and a low-Reynolds number - turbulent model, have been solved using an ADI scheme with preconditioned Chakravarthy-Osher TVD[31].

IV. Flow Transient Mechanism from Booster to Sustainer

In the physical configuration used for simulations, the cowl radius R_c is 3.4 *cm* and the length of the inlet diffuser is 40.12 c_m. The combustion chamber measures 38.93 *cm* in length and 7,786 *cm* in radius, and the nozzle measures 8.16 *cm* in length. The throat area of the inlet diffuser *Ati* is fixed at 0.615 *Ac*, and that of the exhaust nozzle A_{tn} at 1.322 A_c, where $Ac(=R_c^2)$ is the cowl area (see Fig. 2). The inlet flow conditions are set at the inlet design condition, which has a Mach number of 2.1, temperature of 271.91 *K*, pressure of 0.74 *atm.*, and altitude 2.5 km.

To comprehensively analyze the initial transient mechanism, two geometrical domains are considered. One consists of the inlet and the booster combustion chamber, separated by the inlet port cover (Fig. 2a), and the other is the entire ramjet engine without the port cover (Fig. 2b). Computations are carried out sequentially on the two different regimes (first with the port cover, then without it), as described in the following sections.

The computational domain is divided into four zones (see Fig. 3). Zone 1 is the external flow region, zone 2 is the supersonic diffuser region, and zones 3 and 4 make up the combustion chamber region. The dimensions of the grid points for each zone are 8850, 21460, 17060, and 17050, respectively.

A. Flow Structure With the Inlet Port Cover in Place

During rocket operation, the inlet diffuser is isolated from the combustor by a port cover at the interface as depicted in Fig. 2a, and acts as a long coaxial cavity. The combustion chamber functions as a conventional rocket motor. Calculation is first carried out to determine the flow structure in the case of placing the inlet port cover. The computational domain is composed of two blocks for inlet flow calculation (Fig. 2a). The air approaching the ramjet engine at supersonic speed passes several oblique shocks and is stagnated at the front of the port cover.

The wedge-shaped supersonic diffuser consists of two ramps which turn the airflow and introduce oblique shocks which decelerate the flow. Since the pressure behind the terminal shock keeps increasing due to the closed end of the inlet, the terminal shock is pushed out toward the inlet cowl to adjust to the flow conditions of the front zone and the

aft zone of the terminal shock. The terminal shock is expelled from the inlet cowl, moves toward the vertex of the ram core, and finally forms a bow shock detached from the cowl lip due to the formation of a large subsonic region, accompanied by the reversed subsonic flow. Fig. 4 shows the detailed flow fields near the cowl. Two oblique shocks occurred due to the discontinuity in the surface of the ram core to hit the bow shock and make it much steeper. The interaction of the bow shock and a boundary layer forms a Lambda shock on the ram surface. Since the bow shock makes the flow subsonic near the ram core and the shock wave is detached, the incoming air spills over the inlet cowl. This flow is drastically expanded over the inlet cowl. The flow spilled along the cowl surface cannot keep following this surface which is turning almost 180 degrees. Thus, a separation bubble appears on the front outside surface of the cowl-lip which looks like the transient bubble on the transonic airfoil surface at high angles of attack. Two kinds of slip lines are formed, since the bow shock causes a change in entropy. Fig. 5 shows the schematic of these complicated flow structures. During the rocket boost phase, the stagnation pressure of the ram air at the front of the inlet port cover is balanced on the other side by the chamber pressure produced by the burning rocket propellant. At the end of the boost phase, the rocket propellant is almost exhausted except for some slivers, and the pressure in the combustion chamber decays. During this period, the inlet port cover is forced into the combustion chamber as the inlet ram air pressure exceeds the residual pressure of the chamber.

B. Transient Flowfield on Opening the Inlet Port Cover

Fig. 2b and 3b show the physical and computational domains, respectively, for simulating the transient flow field of an entire ramjet engine upon opening of the inlet port cover. The computational domain consists of four blocks.

By using the results of the previous section as initial conditions, the calculation continues to analyze the initial transient phenomena without the inlet port cover. The operating time is set to zero at the moment of burst the port cover. To better observe the transition phenomena, Figs. 6 though Fig. 8 present three different (time) sequences of the transitional ramjet flow. Fig. 6 shows the behavior of the bow/terminal shock and the evolution of the terminal shock train. Fig. 7 shows the generation/movement/reformation of the vortices and reversed flow regions in the combustor. Fig. 8's series show the temperature contours as the incoming cold ram air interacts with the residual hot gases in the chamber. The flow patterns are specifically discussed in this section.

B.1 The Terminal Shock Train

As shown before, a detached bow shock is formed outside the inlet cowl, and this bow shock functions also a terminal shock. After the inlet port cover is opened, this bow shock is weakened and disappears as the ram air flows into the combustion chamber. The bow shock is changed to a normal shock and is swallowed into the inlet cowl. Since the oblique shock reflecting from the cowl lip and the terminal shock are matched on the ram core surface, a thick boundary layer is observed (Fig. 6b). The terminal shock keeps moving toward the combustion chamber and

is smeared in the inlet (Fig. 6d). This smeared shock is reformed due to the acoustic wave reflected from the nozzle (Fig. 6e), and disappears again in the inlet (Fig. 6f).

As the ram air penetrates further into the chamber, the terminal shock is not reformed anymore. Instead of a terminal shock, a series of diamond shocks are formed like an extremely overexpanded supersonic jet (Fig. 6g). It is noted that the ramjet fuel might be injected into combustor before the supersonic ram air reaches the nozzle wall. Otherwise it may be too difficult to ignite the ramjet fuel since the sufficient fuel to ignite ramjet fuel can not penetrate into the recirculation zone, the location of the ignition of ramjet fuel. The streamline patterns (Fig. 7), also, support this claim since fuel streak follows the streamline.

B.2 The Generation/ Movement/ Reformation of Vortex

On opening the inlet port cover, the stagnated ram air suddenly expands, and a small vortex is generated just upstream of the dump plane of the combustion chamber (Fig. 7a). This small vortex moves to the corner of the combustion chamber, and a recirculation zone is formed near the backward step of the chamber (Fig. 7b). The recirculation zone grows as the ram air penetrates into the combustor, and the core of the recirculation zone also moves toward the nozzle. As the ram air penetrates into the chamber, its pressure decreases and the air is overexpanded. The ram air separates and other vortices are reformed on the upper and/or center region of the inlet (Figs. 7d through 7f). These vortices shrink and expand like unsteady bubbles under high-pressure conditions, which generates acoustic waves and pushes them into chamber. Fig. 9 shows a snapshot of the vorticity distribution in the entire ramjet engine at the same time as in Fig. 9c (at $t = 1.95$ msec). A sequence of vorticity distributions is presented for the combustor region in Figs. 9b through 9f. These plots clearly show the presence of strong vortices in the inlet boundary layer and the supersonic shear layer extending from the edge of the backward-facing step

The vortex within the corner subsonic recirculation zone is too weak to be resolved by these contours. The oscillating inlet flow affects the formation of vortices in the shear layer. These vortices move downstream until they reach the convergent walls of the nozzle, whereupon some of the vortical fluid is convected back upstream by the recirculation zone near the chamber wall. In the shear layer, they become highly stretched due to the high strain rate of the mean flow there. It is noted that this strain rate decreases in the case of chemically reacting flow, since the mean supersonic flow near the backward-facing step becomes subsonic due to the reformation of the terminal shock by the forcing of combustor pressure.

B.3 The Interaction of the Cold Ram Air and the Hot Booster Gas

Once the port cover has been opened, the highly compressed, stagnated, and cold ram air pushes the hot booster gases toward the nozzle and expands into the recirculation zone (Fig. 8). The expansion of the ram air aids in the spreading of fuel into the recirculation zone (Fig. 10a). As the ram air spreads into the chamber, hot gas is washed out through the nozzle. Although the ram air displaces much of the residual booster gas, some hot gas still remains in the recirculation zone

(Fig. 8g). Since the pressure near the backward step is relatively high as hot gas in the center region of the chamber is washed out, the hot gas remaining near the backward-facing step starts to roll up with the cold ram air toward the center region of the chamber. This roll-up of the hot gas makes the temperature gradient of the chamber more uniform, which promotes stable ignition. However, ignition should be carefully timed since the roll-up of the hot gas initially creates a local hot spot in the chamber, which may cause some overshoot of combustor pressure and dynamic flame shedding, making the ignition unstable, as detailed further in Part II.

From the above observations, three potentially positive mechanisms to assist the stable ignition of ramjet fuel are summarized. First, the expansion of the ram air enhances spreading of fuel into the recirculation zone. Second, even after introduction of the cold ram air into the chamber, some high-temperature gas still remains near the backward step to supply energy to ignite the fuel. Finally, the relatively uniform temperature in the chamber due to roll-up of the hot gas at the backward step is conducive to stable ignition.

V. Summary and Conclusions

The flow transient mechanism of an IRR system was investigated using the dual time stepping numerical algorithm with preconditioning method. The conservation equations, including a low-Reynolds number - turbulence model, were solved using an ADI scheme with preconditioned Chakravarthy-Osher TVD.

To analyze the flow transitions from booster to sustainer, the computational geometry consists of the entire IRR engine, including the inlet, the combustion chamber, and the exhaust nozzle.

The calculations for the rocket booster phase, in which the inlet port cover is closed, show that the terminal shock train reflected from the port cover forms a large detached bow shock outside the inlet. On opening the inlet port cover, to begin the ramjet phase, the terminal shock is smeared out and the flow throughout the entire engine becomes supersonic. A terminal shock train, generation/ movement/ reformation of vortices, and the dynamic interaction of cold ram air and the hot gas of the booster are observed during the penetration of ram air into the combustion chamber. These dynamic mechanisms enhance uniform distributions of gas temperature and fuel in the combustion chamber. However, ignition should be carefully timed since the roll-up of the hot gas initially creates a local hot spot in the chamber, which may cause some overshoot of combustor pressure and dynamic flame shedding, making the ignition unstable, as detailed further in the next paper.

The oscillation and peristalsis of the supersonic core in the inlet periodically drive a series of vortices. Also the periodic evolving of a ring vortex is observed in the combustion chamber.

REFERENCES

1. Waltrup, P. J., White, M. E., and Gravlin, E. S., History of U.S. Navy Ramjet, Scramjet, and Mixed Cycle Propulsion Development, *AIAA Paper* 96-3152, 1996.
2. Myers, T. D., Integral Boost, Heat

Protection, Port Covers and Transition, *AGARD*-LS-136, pp. 4-1~20, 1984.
3. Chen, C. P., Sajben, M., and Kroutil, J. C., Shock-Wave Oscillations in a Transonic Diffuser Flow, *AIAA Journal*, Vol. 17, No. 10, 1979, pp. 1076~1083.
4. Bogar, T. J., Sajben, M., and Kroutil, J. C., Characteristic Frequencies of Transonic Diffuser Flow Oscillations, *AIAA Journal*, Vol. 21, 1983, pp. 1232~1240.
5. Salmon, J. T., Bogar, T. J., and Sajben, M., Laser Doppler Velocimeter Measurements in Unsteady, Separated, Transonic Diffuser Flows, *AIAA Journal*, Vol. 21, No. 12, 1983, pp. 1690~1697.
6. Sajben, M., Bogar, T. J., and Kroutil, J. C., Forced Oscillation Experiments in Supercritical Diffuser Flows, *AIAA Journal*, Vol. 22, No. 4, 1984, pp. 465~474.
7. Sajben, M., Bogar, T. J., and Kroutil, J. C., Experimental Study of Flows in a Two-Dimensional Inlet Model, *Journal of Propulsion and Power*, Vol. 1, No. 2, 1985, pp. 109~117.
8. Bogar, T. J., Sajben, M., and Kroutil, J. C., Response of Supersonic Inlet to Downstream Perturbations, *Journal of Propulsion and Power*, Vol. 1, No.2, 1985, pp. 118~125.
9. Bogar, T. J., Structure of Self-Excited Oscillations in Transonic Diffuser Flows, *AIAA Journal*, Vol. 24, 1986, pp. 54~61.
10. Culick, F. E. C. and Rogers, T., The Response of Normal Shocks in Diffusers, *AIAA Journal*, Vol. 21, No. 10, 1983, pp. 1382~1390.
11. Yang ,V. and Culick, F. E. C., Analysis of Unsteady Inviscid Diffuser Flow With a Shock Wave, *Journal of Propulsion and Power*, Vol. 1, No. 3, 1985, pp. 222~228.
12. Hsieh, T., Wardlaw, A. B., Collins, P., and Coakley, T. J., Numerical Investigation of Unsteady Inlet Flow Fields, *AIAA Journal*, Vol. 25, No. 5, 1987, pp. 75~81.
13. Hsieh, T., Bogar, T. J. and Coakley, T. J., Numerical Simulation and Comparison with Experiment for Self-Excited Oscillations in a Diffuser Flow, *AIAA Journal*, Vol. 25, No. 7, 1987, pp. 936~943.
14. Oh, J. Y., Numerical Study of Steady and Oscillatory Flow Structures in an Axisymmetric Supersonic Inlet, *Ph.D. Thesis*, The Pennsylvania State University, University Park, PA, August 1994.
15. Schadow, K. C., Crump, J. E., and Blomshield, F. S., Combustion Instability in a Research Dump Combustor: Inlet Shock Oscillations, *Proceedings of 18th JANNAF Combustion Meeting*, 1981.
16. Abouseif, G. E., Keklak, J. A., and Toong, T.Y., Ramjet Rumble: The Low Frequency Instability Mechanism in Coaxial Dump Combustors, *Combustion Science and Technology*, 1984, pp. 83~108.
17. Yang, V. and Culick, F. E. C., Analysis of Low Frequency Combustion Instabilities in a Laboratory Ramjet Combustor, *Combustion Science and Technology*, Vol. 45, 1986, pp. 1~45.
18. Yang, V. and Culick, F. E. C., Nonlinear Analysis of Pressure Oscillations in Ramjet Engines, *AIAA Paper* 86-0001, 1986.
19. Kailasanath, K., Gardner, J. H., Oran, E. S., and Boris, J. P., Effects of Energy Release on High-Speed Flows in an Axisymmetric Combustor, *AIAA Paper* 89-0385, 1989.
20. Menon, S. and Jou, W.-H., Large-Eddy

Simulations of Combustion Instability in an Axisymmetric Ramjet Combustor, *Combustion Science and Technology*, Vol. 75, 1991, pp. 53~72.

21. Menon, S., Active Combustion Control in a Ramjet Using Large-Eddy Simulations, *Combustion Science and Technology*, Vol. 84, 1992, pp. 51~79.
22. Bauwens, L. and Daily, J. W., Flame Sheet Algorithm for Use in Numerical Modeling of Ramjet Combustion Instability, *Journal of Propulsion and Power*, Vol. 8, No. 2, 1992, pp. 264~270.
23. Hsieh, S. and Yang, V., A Unified Analysis of Unsteady Flow Structures in a Supersonic Ramjet Engines, *AIAA Paper* 97-0396, 1997.
24. Sung, H.-G., Hsieh, S., and Yang, V., Flow and Ignition Transients in an Integrated Ramjet Engine: from Booster to Sustainer , 37th AIAA Aerospace Science Meeting and Exhibit, AIAA 99-0089, 1999.
25. Sung, H.-G., Hsieh, S., and Yang, V., Transient Operation of an Integrated Ramjet Engine: from Booster to Sustainer, PERC 11th Annual Symposium on Propulsion, Nov. 1999.
26. Sung, H.-G., Dynamic Interference's between an Inlet Terminal Shock and Flame in an Integrated Ramjet Engine , International Workshop on Hypervelocity and Aerospace Propulsion, Jan., 2000.
27. Webster, F. F., Ramjet Development Testing: Which Way is Right? *Journal of Propulsion and Power*, Vol. 5, No. 5, 1989, pp. 565~576.
28. Jones, W. P. and Launder, B. E., The Calculation of Low-Reynolds Number Phenomena with a Two-Equation Model of Turbulence, *International Journal of Heat and Mass Transfer*, Vol. 16, 1973, pp. 1119~1130.
29. Shih, T. H. and Lumley, J. L., Kolmogov Behavior of Near-Wall Turbulence and Its Application in Turbulence Modeling, *NASA* TM-105663, 1992.
30. Yang, Z. and Shih, T. H., New Time Scale Based k- Model for Near Wall Turbulence, *AIAA Journal*, Vol. 31, No. 7, 1993, pp. 1191~1197.
31. Chakravarthy, S. R. and Osher, S., A New Class of High Accuracy TVD Schemes for Hyperbolic Conservation Laws, *AIAA Paper* 85-0363, 1985.

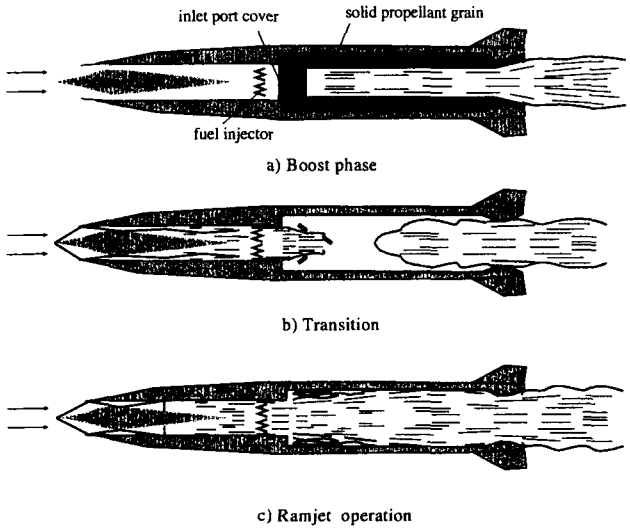

Fig. 1. Conceptual diagram of a coaxial integrated rocket ramjet engine during the transition from booster to ramjet sustainer.

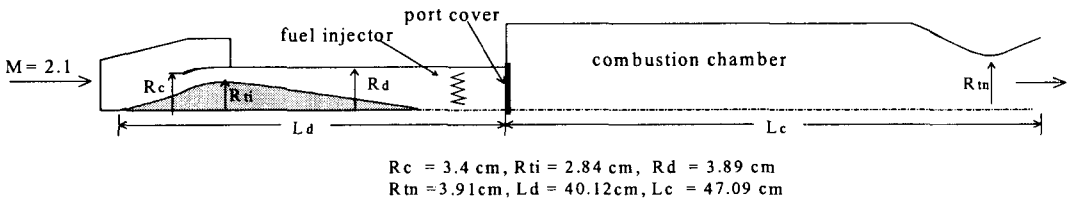

Rc = 3.4 cm, Rti = 2.84 cm, Rd = 3.89 cm
Rtn = 3.91cm, Ld = 40.12cm, Lc = 47.09 cm

a) Physical domain with an inlet port cover in place

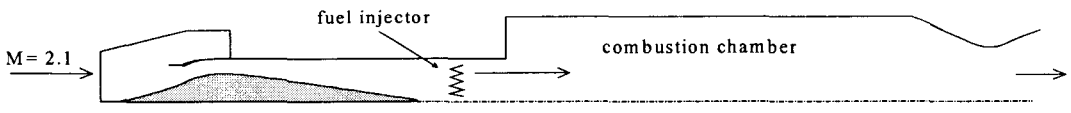

b) Physical domain in case of opening an inlet port cover

Fig. 2 Schematic of physical geometry both with and without an inlet port cover

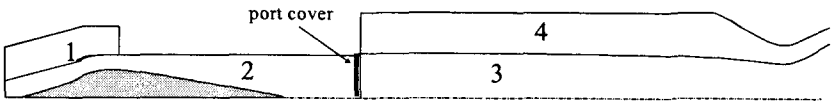

a) Computational domain with an inlet port cover in place

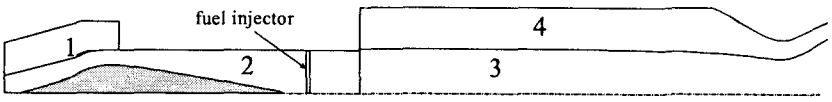

b) Computational domain in case of opening an inlet port cover

Fig. 3. Schematic of computational domain both with and without an inlet port cover.

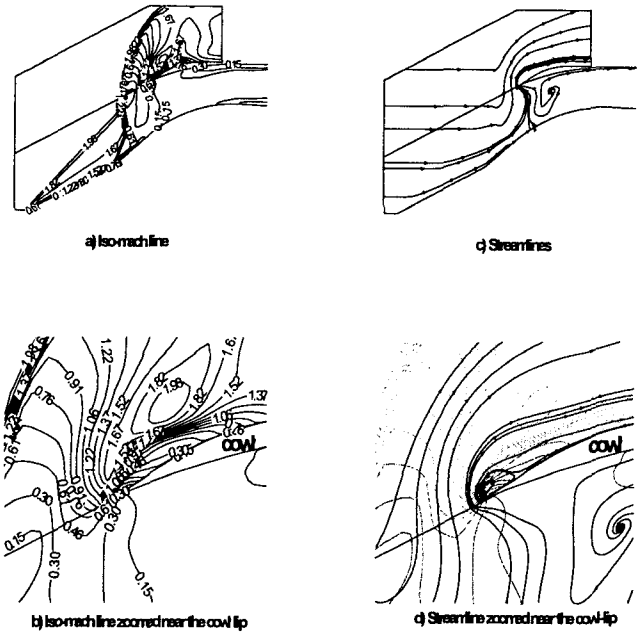

Fig. 4. Mach number contours and streamline pattern near the cowl

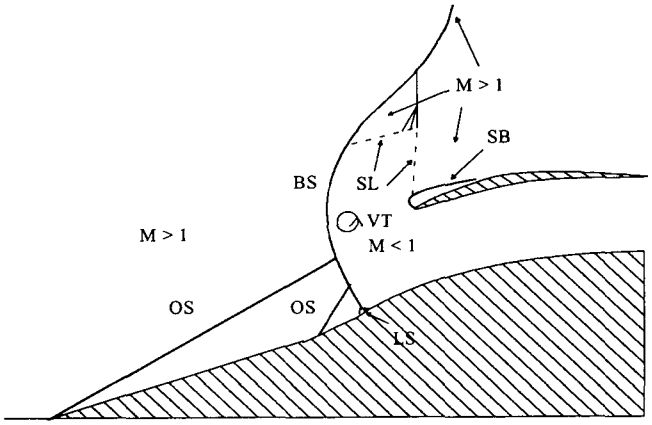

Fig. 5. Schematic of the flow fields near the cowl lip with an inlet port cover

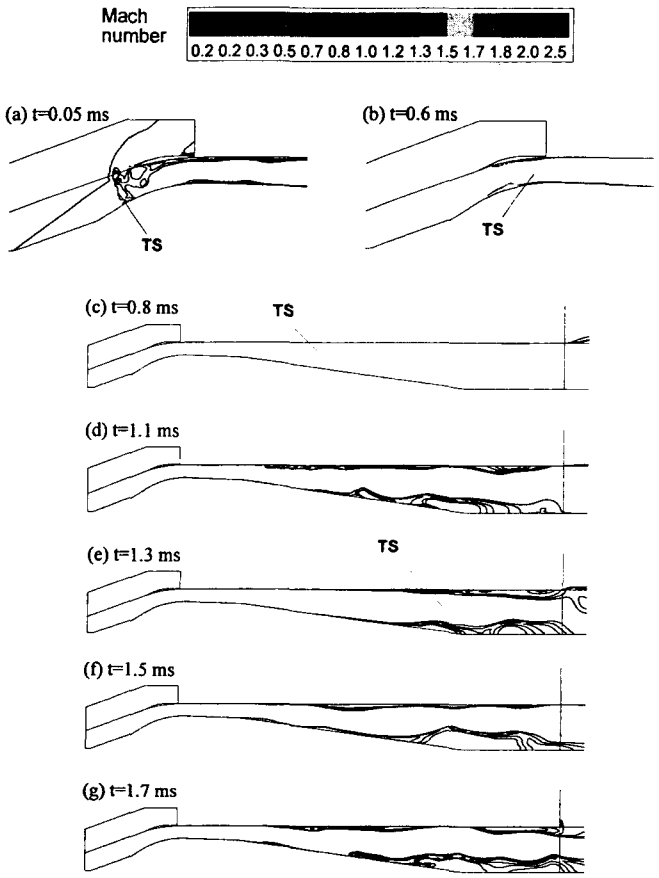

Fig. 6. Time evolution of terminal shock (TS) in the Mach number field on opening the inlet port cover.

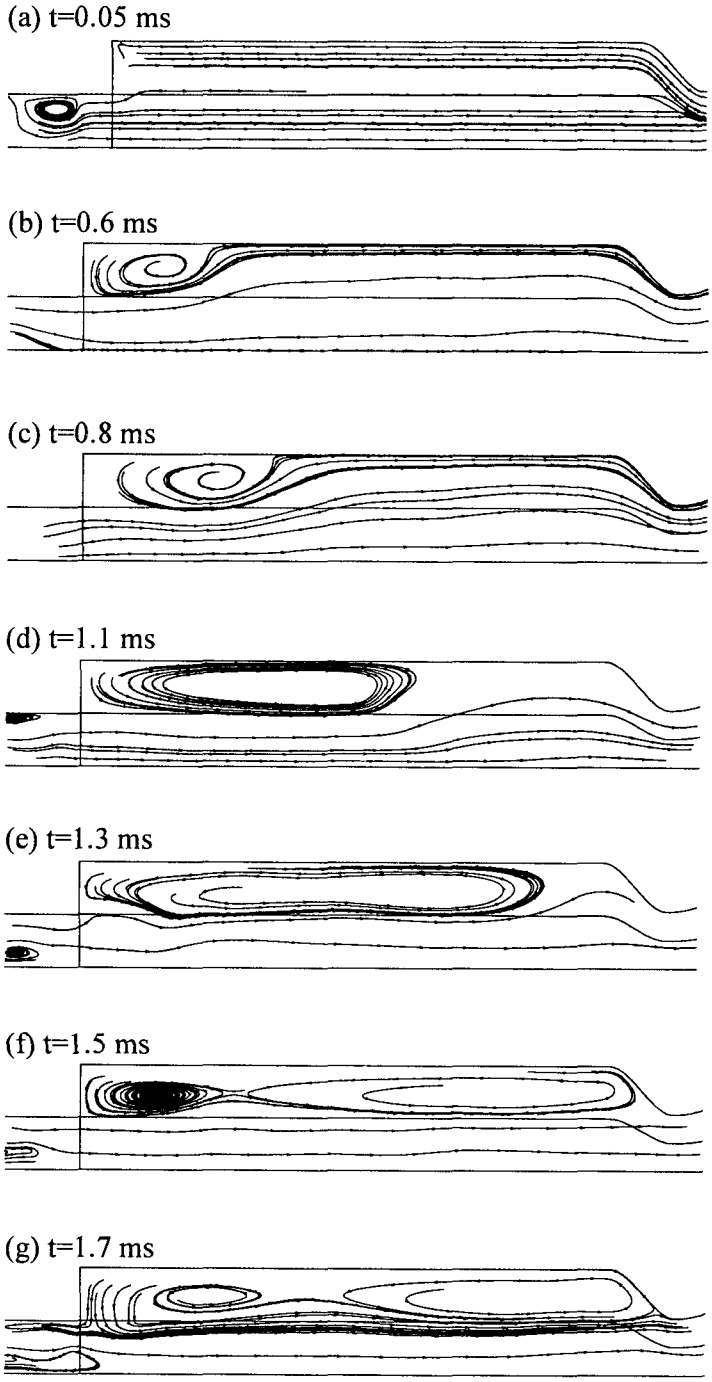

Fig. 7. Time evolution of a streamline pattern on opening the inlet port cover

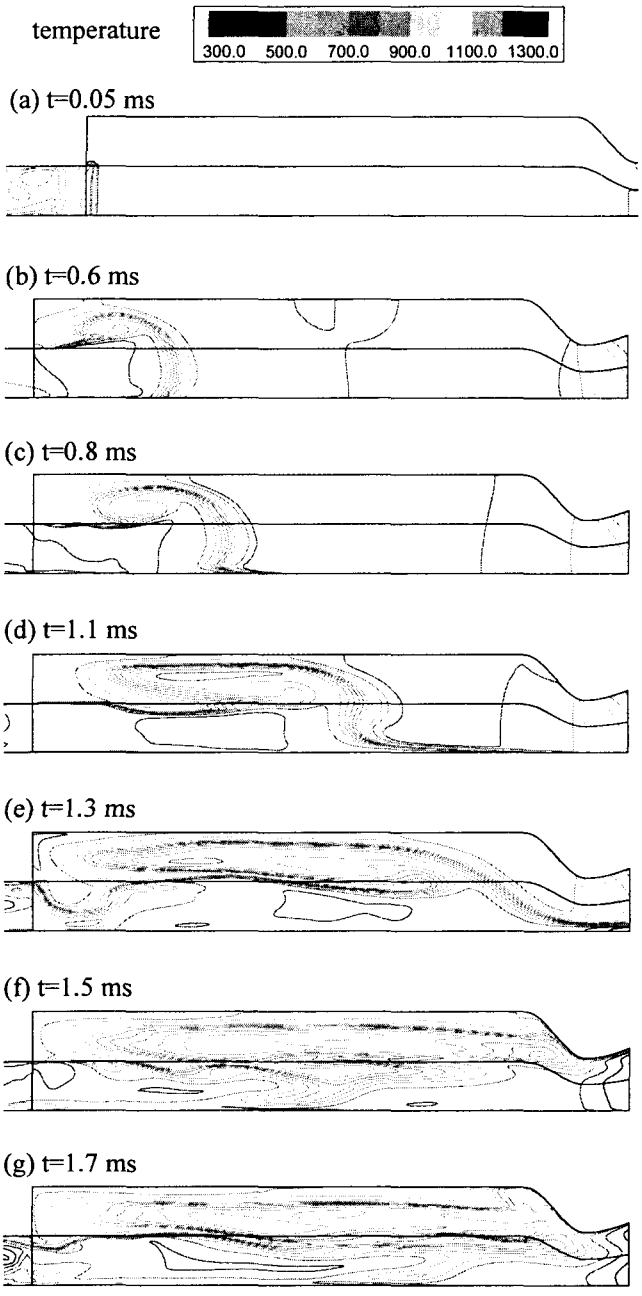

Fig. 8. Time evolution of the distribution of temperature on opening the inlet port cover

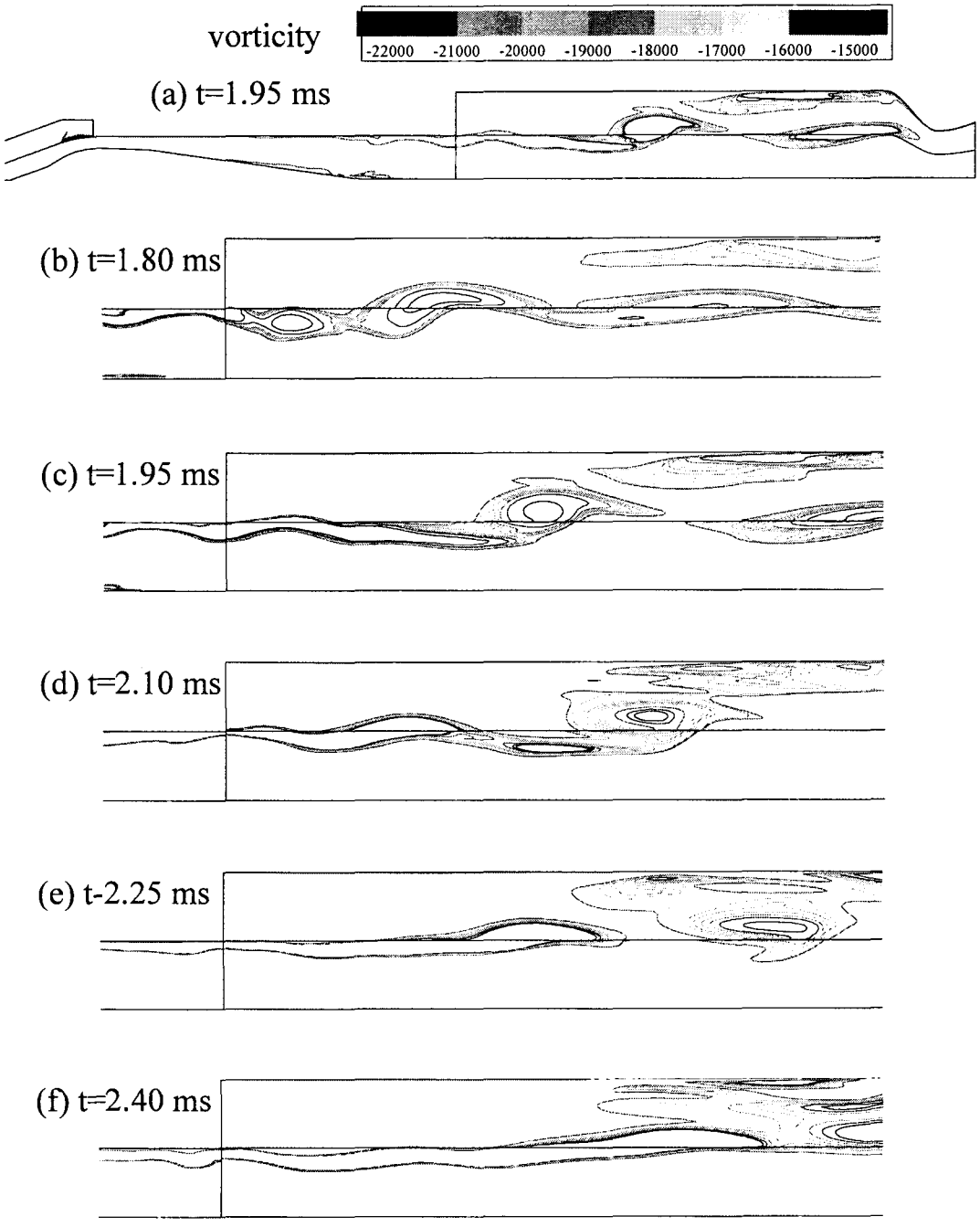

Fig. 9. Time evolution of a ring-vortex

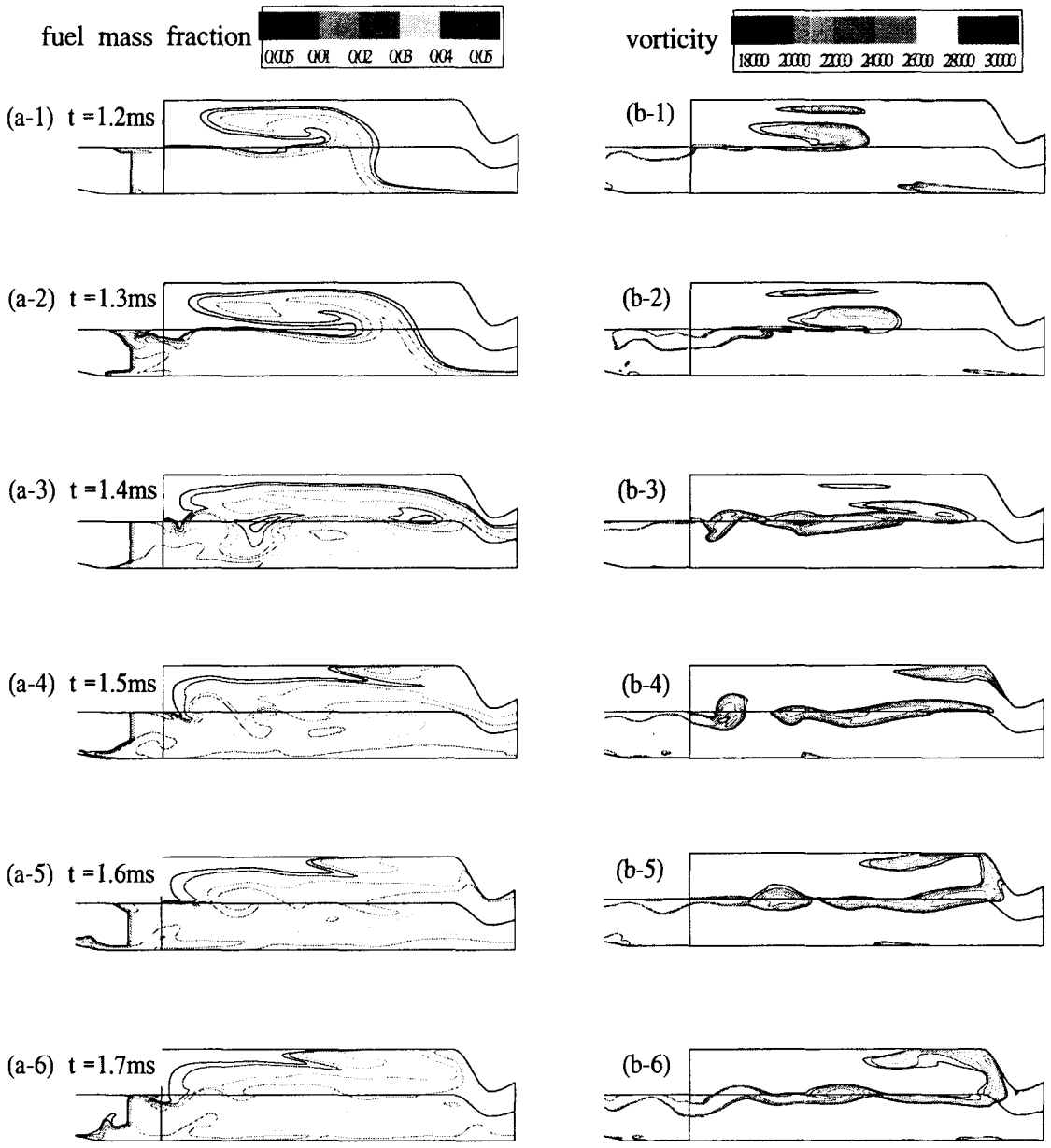

Fig. 10. Ramjet fuel spreading and vorticity fields before ignition of the ramjet fuel